buildings

MDPI

Article

An Assessment of the Seismic Performance of EC8-Compliant CBFs Taking into Account the Role of Soil: A Case Study

Melina Bosco *, Angela Fiamingo, Maria Rossella Massimino and Pier Paolo Rossi

Department of Civil Engineering and Architecture, University of Catania, Via Santa Sofia 64, 95123 Catania, Italy; angela.fiamingo@unict.it (A.F.); maria.massimino@unict.it (M.R.M.); pierpaolo.rossi@unict.it (P.P.R.)
* Correspondence: melina.bosco@unict.it

Abstract: Based on criticisms raised in the past by researchers about the effectiveness of the design rules reported in the European seismic code for the design of concentrically braced frames, a new design procedure has been proposed and included in the upcoming version of Eurocode 8. The upcoming version of Eurocode 8 is in the enquiry stage. Hence, it is important to evaluate the effectiveness of the design procedure reported in the code using accurate numerical models and seismic inputs. In the present paper, a four-story building with concentrically braced frames in the chevron configuration is designed according to the upcoming version of Eurocode 8. A seismic performance assessment is carried out by the means of multiple-stripe analyses performed on refined numerical models. The seismic input is defined based on one-dimensional local site response analyses. The numerical analyses prove that the use of local site response analysis to properly account for the soil-filtering effects is of paramount importance, and that the design procedure reported in the upcoming version of Eurocode 8 for chevron concentrically braced frames leads to reasonably low probabilities of exceeding the considered limit states.

Keywords: concentrically braced frames; soil effect; local site response analysis; assessment of seismic response; seismic provisions

check for updates

Citation: Bosco, M.; Fiamingo, A.; Massimino, M.R.; Rossi, P.P. An Assessment of the Seismic Performance of EC8-Compliant CBFs Taking into Account the Role of Soil: A Case Study. *Buildings* **2024**, *14*, 2161. https://doi.org/10.3390/buildings14072161

Academic Editor: Eric M. Lui

Received: 16 June 2024
Revised: 6 July 2024
Accepted: 12 July 2024
Published: 14 July 2024

Copyright: © 2024 by the authors. Licensee MDPI, Basel, Switzerland. This article is an open access article distributed under the terms and conditions of the Creative Commons Attribution (CC BY) license (https://creativecommons.org/licenses/by/4.0/).

1. Introduction

Steel concentrically braced frames are widely used in seismically prone countries. However, in the last decades, several studies have highlighted some criticisms about the design procedure stipulated in Eurocode 8 [1]. In regard to the design of dissipative members, i.e., braces, attention has been mainly focused on evaluating the overstrength [1–3] and its distribution along the height of the building [4,5]. Regarding non-dissipative members, instead, some criticisms have been raised about the effectiveness of the rules for the application of the capacity design principles in preventing the yielding or buckling of columns [6–11]. Indeed, based on the results of nonlinear dynamic analyses, it has been shown that the rules for the application of the design capacity principles given in Eurocode 8 underestimate the axial forces in columns and virtually neglect bending moments in the same members. With specific regard to concentrically braced frames in the chevron configuration, attention has also been focused on the importance of the flexural stiffness of the beam of the braced bay [1,6,11] in order to promote yielding of the tensile brace. Still, in regard to the braced beams, it has been proven that the Eurocode 8 provisions underestimate the unbalanced vertical force transmitted by the braces when the brace in tension yields and the brace in compression is in its post-buckling range of behavior [1,11]. This underestimation often leads to premature yielding of the beam, which is considered to be a fragile member in Eurocode 8. Previous experimental tests and numerical studies, however, have highlighted that moderate yielding in the beam is not detrimental to the nonlinear response of the frame [12]. A key aspect in the seismic response of braced frames is also related to the design of connections at the end of the braces. It has been pointed out

that the strength and stiffness of the gusset plate connection must be adequate to promote the expected resistance of the brace, but that a very high strength and stiffness promote the concentration of the inelastic deformation along a short length of the brace and cause early brace fracture [13].

The main criticisms raised by researchers have been addressed in the upcoming version of Eurocode 8 [14]. Since the upcoming version of Eurocode 8 is currently in the enquiry stage, it is important to evaluate the effectiveness of the design procedures reported in the code using accurate numerical models of structure and seismic input. In regard to the proper modeling of the cyclic response of braces, D'Aniello et al. [15] carried out numerical analyses considering braces characterized by different values of out-of-straightness imperfection, whereas Silva et al. [16] and Bosco [17] pointed out the effects provided by different modeling strategies for the connections at the ends of braces. Montuori et al. [18], instead, analyzed the effects of the gravity column on the seismic design of CBFs.

An aspect that is often neglected in studies dealing with concentrically braced frames is the Dynamic Soil–Structure Interaction (DSSI), i.e., the process in which the response of the soil influences the motion of the structure, and the motion of the structure influences the response of the soil [19].

The soil modifies the bedrock motion, so the amplitude and frequency content of the resulting surface ground motion can become disadvantageous for some structures. The unique value of the soil factor provided by the Italian Seismic Code [20] for soil type B (equivalent shear wave velocity, V_s, in the range from 360 to 800 m/s) is too rough and does not allow for a deep evaluation of the soil-filtering influence. Secondly, the soil and foundation alter the vibrational characteristics of structures and can shift the period to a spectral region characterized by a higher amplification [21].

To more comprehensively take into account the soil-filtering influence, local site response analyses are necessary [22,23] and a more refined subdivision of soil types according to the soil shear wave velocity is desirable [24], as demonstrated by the results reported below. Additionally, the amplification and de-amplification of the seismic input due to specific soil conditions (geometry, physical properties, nonlinearity) are key aspects when evaluating the seismic responses of structures [25–29]. Local site response analyses consider the specific soil conditions and allow us to properly evaluate the soil-filtering effects.

Furthermore, the effects of the soil–foundation flexibility have recently been considered in the evaluation of the seismic collapse performance of low-rise split X-braced frames [30].

In the present paper, a four-story building with concentrically braced frames in the chevron configuration is designed according to the upcoming version of Eurocode 8. Its seismic performance is assessed by the means of multiple-stripe analyses carried out on accurate numerical models that also account for soil through distributed nonlinear springs and dampers, computed considering the predominant period of the flexibly supported structure configuration. Furthermore, to simulate the soil–structure interaction, the seismic input is first generated at the base of the foundation by the means of local site response (LSR) analyses in order to consider the soil-filtering effects [31–33]. Then, the dynamic response of the structure supported on nonlinear springs and dampers is evaluated ("sub-structure" approach [34] based on the Beam on Nonlinear Winkler Foundation, BNWF).

2. Design Procedure for Concentrically Braced Frames according to Upcoming Version of Eurocode 8

The upcoming version of Eurocode 8 provides a design procedure that is applicable to concentrically braced frames independently of the geometric configuration of the braces. The main steps of this procedure for buildings in the high ductility class (DC3) are summarized here.

Concentrically braced frames are designed based on a force-based design procedure. The maximum value of the behavior factor that can be used, independent of the geometric

configuration of the braces, is equal to 4.0. This value is relatively larger than that provided by the current version of Eurocode 8 for chevron braced frames, i.e., 2.5.

Braces are designed so that the buckling resistance $N_{b,Rd}$ is larger than the axial force N_{Ed} determined as the sum of the axial forces provided by gravity loads ($N_{Ed,G}$) and seismic actions ($N_{Ed,E}$) in the seismic design situation. To account for the connections at the ends of braces, the buckling length of the braces is calculated as 0.8 times the centerline-to centerline length of the brace. The braces of the top story are designed to remain in the elastic range of behavior. Hence, the cross-section of the braces of the top story is such that the buckling resistance of these members is larger than the axial force $N_{Ed,E}$ amplified by the behavior factor. To promote a global dissipative behavior, with the exception of the top story, the ratio of the maximum to minimum overstrength of the braces Ω has to be lower than 1.25. To this end, the overstrength is calculated as the ratio of the buckling resistance $N_{b,Rd}$ to the design axial force $N_{Ed,E}$.

Beams and columns should be designed to sustain axial forces and bending moments determined according to three different scenarios.

In the first scenario, the axial forces and bending moments are determined as the sum of the contribution provided by the gravity loads in the seismic design situation ($N_{Ed,G}$, $M_{Ed,G}$, and $V_{Ed,G}$) and the contribution provided by seismic actions ($N_{Ed,E}$, $M_{Ed,E}$, and $V_{Ed,E}$), amplified to account for the minimum design overstrength of the braces (Ω_d), the material overstrength of steel in the dissipative zone (ω_{rm}), and the hardening of the dissipative zone (ω_{sh}), i.e.,

$$\begin{aligned} N_{Ed} &= N_{Ed,G} + \omega_{rm}\omega_{sh}\Omega_d N_{Ed,E} \\ M_{Ed} &= M_{Ed,G} + \omega_{rm}\omega_{sh}\Omega_d M_{Ed,E} \\ V_{Ed} &= V_{Ed,G} + \omega_{rm}\omega_{sh}\Omega_d V_{Ed,E} \end{aligned} \quad (1)$$

In particular, Ω_d is the minimum of the ratios $N_{pl,Rd}/N_{Ed,E}$ for all the braces, where $N_{pl,Rd}$ is the tension axial resistance of the brace. For concentrically braced frames, ω_{sh} is equal to 1.1, whereas ω_{rm} depends on the steel grade.

In the second scenario, the internal forces provided by seismic actions are calculated considering a free-body distribution of axial forces in both tension and compression diagonals, with the values of the axial forces equal to their expected buckling resistance ω_{rm} $N_{b,Rd}$.

In the third scenario, the internal forces are calculated by equilibrium conditions, considering that the braces under tension forces are fully yielded (axial force equal to ω_{rm} ω_{sh} N_{Rd}) and the braces under compression forces are in the post-buckling range of behavior (axial force equal to 0.3 ω_{rm} $N_{b,Rd}$). In this latter scenario, bending moments are considered in the columns and, in the case of chevron braced frames, bending moments are also considered in the beams. In particular, the bending moments of the beams are caused by the unbalanced vertical force F_v transmitted by the braces; the bending moments in the columns, in the plane of the braced frame, are set as being equal to 0.2 times the plastic moment resistance of the gross section of the column.

Further, the flexural stiffness of the braced beam should not be smaller than 0.2 times the vertical stiffness of the intersecting braces.

Brace connections are designed to resist the axial forces transmitted by the braces (ω_{rm} ω_{sh} N_{Rd}). The buckling resistance of the gusset plates has to be larger than the buckling resistance of the braces (ω_{rm} $N_{b,Rd}$). Further, gusset plate connections should be designed to accommodate brace buckling under repeated cyclic loading. To this end, a $2t_p$ to $4t_p$ clearance should be detailed between the end of the brace and the assumed geometric line of the gusset restraints, where t_p is the gusset plate thickness.

A comparison with the relevant provisions of the current version of Eurocode 8 is reported in Table 1. In the same table, the main criticisms raised by researchers are also briefly reported.

Table 1. Modifications introduced in the upcoming version of EC8 for the design of chevron braced frames.

Provision	Current Provision	Criticism	Upcoming Provision
Uniformity of brace overstrength	$\Omega_{max}/\Omega_{min} \leq 1.25$	To fulfill this requirement at the top story, the braces of other stories have to be oversized [4,5]	Braces of the top story are designed to remain in the elastic range of behavior
Ultimate resistance of the brace	$N_u = 0.30\ N_{pl,Rd}$	Ultimate resistance of the brace is overestimated [5,11]	$N_u = 0.30\ N_{b,Rd}$
Bending moment in braced beams caused by unbalanced vertical force F_v of braces	$F_v = (N_{pl,Rd} - N_u)\sin\alpha$	Bending moment is underestimated because of the overestimation of the ultimate resistance of the brace [5,11]	$F_v = (\omega_{rm}\omega_{sh}N_{pl,Rd} - N_u)\sin\alpha$
Flexural stiffness of the braced beam	No provision	A flexible beam prevents the tensile brace from yielding, thus reducing the dissipation capacity [1,6]	Flexural stiffness > 0.2 times the vertical stiffness of the braces
Axial force in columns	$N_{Ed} = N_{Ed,G} + 1.1\gamma_{ov}\ \Omega_{min}\ N_{Ed,E}$	Axial forces are underestimated [6–11]	Axial forces are determined considering 3 different scenarios
Bending moments in columns	Virtually neglected	Buckling of columns occurs under the combined effect of axial forces and bending moments [10,11]	$M_{Ed} = 0.20\ M_{pl}$

More details about the design procedure are given in ref. [14].

3. Case Study

Three four-story steel buildings with concentric braces in the chevron configuration are considered as case studies. The plan layout is shown in Figure 1. Two braced bays sustain the seismic actions along each principal direction. To ensure a torsionally rigid response, braced bays are located along the perimeter of the building and are marked by a double line in Figure 1. The inter-story height h is equal to 4.0 m. The values of permanent (G_k) and variable (Q_k) loads are reported in Figure 1. The story mass is calculated considering the characteristic value of gravity loads and the quasi-permanent value of variable loads. The resulting story mass m is reported in the same figure. The structures belong to consequence class 2.

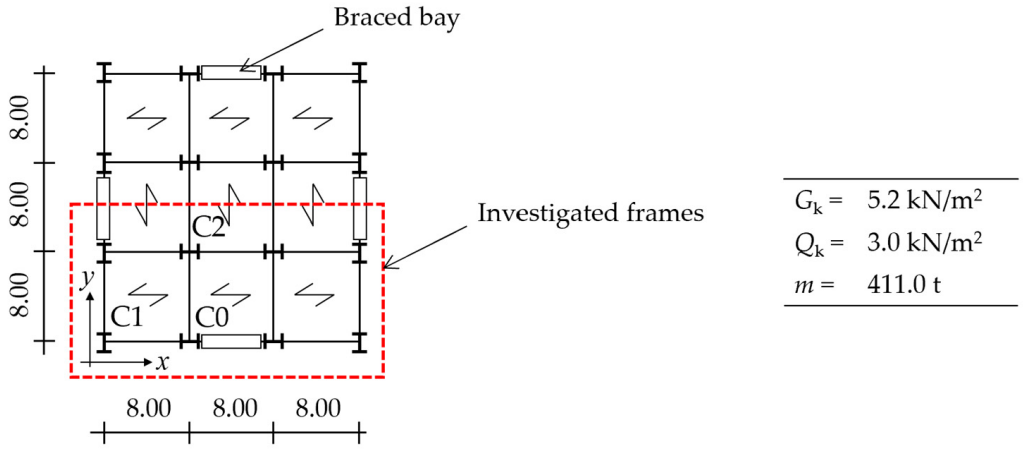


Figure 1. Plan layout of the building and considered loads.

The buildings are located near Siracusa (Sicily) and stand on a deposit of very dense sand that can be classified as soil type B according to Eurocode 8 and the Italian Seismic code [20]. For this soil type, the weighted average value of the shear wave velocity, V_s, is in the range from 360 m/s to 800 m/s. The latter represents a very large range; according to the value of V_s in this range, different soil-filtering effects can be observed. However, Eurocode 8 and the Italian Seismic code suggest a single value of the amplification coefficient S_S. To investigate this aspect, three different sandy soil profiles are considered here, named as soil

B#1 to B#3 in the following. For all the three considered cases, the bedrock lays at 30 m from the surface and a single layer of soil is considered with a thickness equal to 30 m. The main geotechnical properties of the three considered soils are reported in Table 2. With reference to rigid soil (i.e., soil type A), the Italian Seismic Code provides the peak ground acceleration (a_g), the maximum spectral amplification factor (F_0), and the period T_C^* corresponding to the beginning of the branch of the spectrum with a constant velocity. Specifically, for the site under investigation and for seismic events with a probability of exceedance of 10% in 50 years, the above values are equal to 0.279 g, 2.28, and 0.43 s, respectively.

Table 2. Main geotechnical properties of the soil.

Soil Parameter	Soil B#1	Soil B#2	Soil B#3
Shear wave velocity V_s	400 m/s	550 m/s	700 m/s
Bulk unit weight γ_s	17.5 (kN/m^3)	18.5 (kN/m^3)	20.0 (kN/m^3)
Angle of shear strength φ'	37°	40°	43°
Cohesion c'	0.0 kPa	0.0 kPa	0.0 kPa
Modulus of subgrade reaction k_{1s} [1]	100 N/cm^3	225 N/cm^3	350 N/cm^3

[1] determined with a load test on a square plate of side b = 30 cm.

Based on the provisions provided by the Italian Seismic code, the stratigraphic amplification coefficient S_S of soil type B is calculated as:

$$S_S = 1.4 - 0.4F_0\, a_g = 1.146 \quad (2)$$

3.1. Design of the Structure in Elevation

Dissipative members are designed based on the internal forces provided by a modal response spectrum analysis. The maximum value of the behavior factor allowed by the code, i.e., 4.0, is used to derive the design spectrum. A simplified model consisting of pinned braces is used to evaluate the design internal forces. Further, pinned beam-to-column connections are considered. Due to the in-plane symmetry of the structure, a 2D model of half the building is considered. Hollow square cross-sections made of steel grade S355 are used for the braces. The cross-sections and steel grades selected for the braces, braced beams, and columns are reported in Table 3

Table 3. Cross-section of members belonging to the braced frame.

Story	Braces	Beams	Columns
4	S150 × 8 **	HEB 500 *	HEA 300 *
3	S115 × 6 **	HEB 550 **	HEA 300 *
2	S120 × 7 **	HEB 550 **	HEB 320 **
1	S120 × 8 **	HEB 550 **	HEB 320 **

* Steel grade S235, ** Steel grade S355.

HSS members are joined to the gusset plate by means of four fillet welds. The weld throat a is equal to the minimum value between the thickness of the brace cross-section and 6 mm. The length of the fillet welds is fixed so as to resist the axial forces transmitted by the braces. The effective width of the gusset plate W is defined at the portion of the gusset plate identified by the interception between two 30° lines drawn from the tips of the welds to the end of the brace-to-gusset interface. The thickness t_p of the gusset plate is designed according to Annex E of the upcoming version of Eurocode 8. In any case, t_p is smaller than two times the thickness of the brace cross-section. To allow for out-of-plane brace buckling, a linear clearance equal to 2 t_p is detailed.

3.2. Design of Shallow Foundation

A strip foundation is designed. First, the non-seismic design situation is considered; then, the vertical forces transmitted by the columns to the foundation in the seismic design

situation are evaluated in keeping with the three scenarios discussed in Section 2. For each scenario, the horizontal forces transmitted by the braces of the first story are also determined and used to evaluate the bending moments caused by the eccentricity (H_f–Y_g in Figure 2) between the column base and the centroid of the foundation.

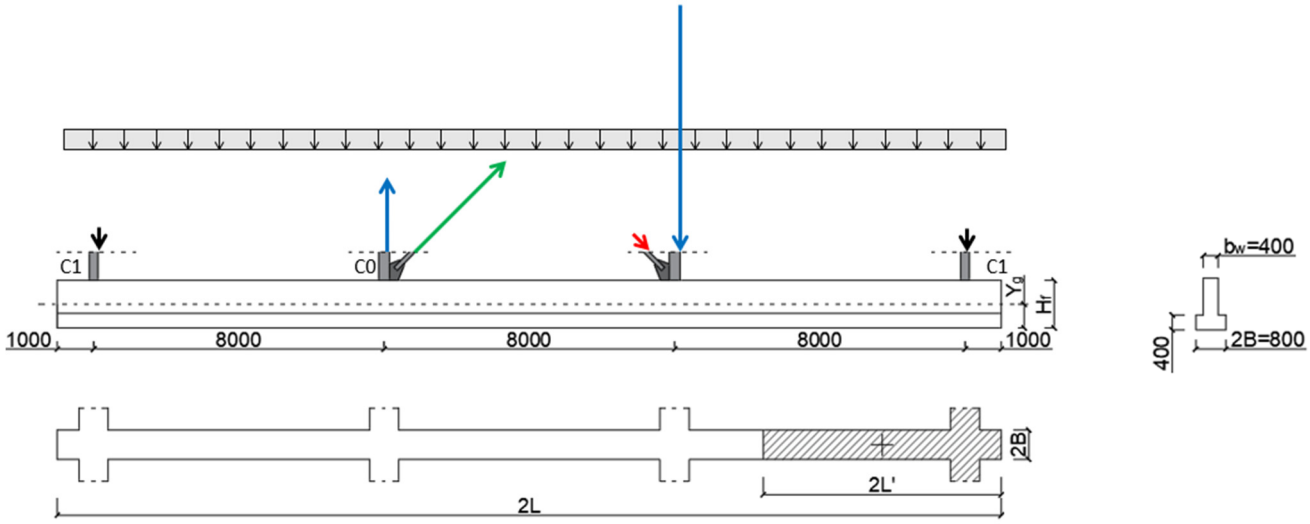


Figure 2. Action on the strip foundation in the design scenario 2 (sizes in mm).

Since the strip foundations are arranged along two orthogonal directions and connected to each other, the vertical force transmitted by the columns is equally shared between the two strip foundations that intersect at the column base in the case of interior and corner columns (columns C2 and C1 in Figure 1). In the case of columns belonging to the braced frame (column C0), instead, 80% of the vertical force is assigned to the strip foundation for which column C0 is a central column and 20% of the vertical force is assigned to the orthogonal strip foundation.

For each scenario, the effective footing length 2*L*′ is calculated to account for the effects of the eccentricity of the loads, and the width of the cross-section 2*B* = 0.80 m is assigned so that the ultimate load capacity, calculated according to the Brinch Hansen theory [35], is greater than the resulting vertical loads.

The width of the web of the cross-section b_w is set as equal to 0.40 m and the height of the cross-section is set as equal to 1.30 m. This value is assigned so that the design value of the maximum shear force $V_{Rd,max}$ that can be sustained by the foundation, limited by crushing of the compression struts, is larger than the design shear force. Finally, the depth of the flange is set as equal to 0.40 m.

Longitudinal rebars and stirrups are calculated based on the internal forces derived by an analysis in which the strip foundation lays on Winkler soil and the soil properties reported in Table 2 are considered.

4. Seismic Input

For the site under investigation, studies carried out by the National Institute of Geophysics and Volcanology (INGV) provide the seismic hazard on stiff soil (soil type A). In particular, the spectral accelerations corresponding to periods of vibration T_i equal to 0.0, 0.10, 0.15, 0.20, 0.30, 0.40, 0.50, 0.75, 1.00, 1.50, and 2.00 s are provided for nine probabilities of exceedance P_{VR}, ranging from 81% to 2% in 50 years. The above probabilities of exceedance correspond to return periods T_R equal to 30, 50, 72, 100, 140, 200, 475, 1000, and 2500 years. For each period of vibration, three percentiles of spectral acceleration (i.e., 16%, 50%, and 84%) are given. Based on the procedure presented in [36], spectral accelerations corresponding to probabilities of exceedance P_{VR} different from those considered by INGV

are derived and, for each considered P_{VR}, a suite of 50 accelerograms is generated by the SIMQKE computer program [37].

Accelerograms to be used as seismic inputs for the three soils under investigation (B#1 to B#3) are determined based on one-dimensional local site response analyses carried out by means of the STRATA software (version 0.2.0) [38]. A different value of the effective strain ratio (*ESR*) is calculated for each suite of accelerograms as a function of the expected moment magnitude M_W:

$$ESR = \frac{M_W - 1}{10} \quad (3)$$

The values of M_W are assigned to each suite of ground motions based on the seismic hazard disaggregation study reported by INGV. The relation proposed by Darendeli and Stokoe [39] for sandy soils is used to relate the shear modulus (G/G_0) and the damping ratio (D) to the shear strain, in order to take into account soil nonlinearity. Finally, the outcrop option is considered (Figure 3).

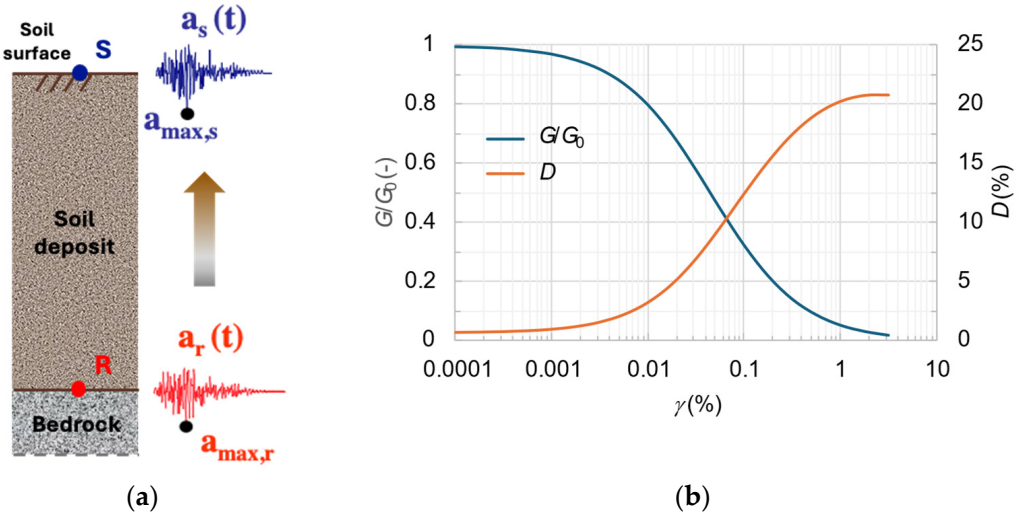


Figure 3. One-dimensional local site response analysis: (**a**) scheme and (**b**) Darandeli and Stokoe curves [34].

As an example, the spectra of the suite of accelerograms obtained for the three considered soils are reported in Figure 4, with reference to return periods equal to 200 years and 475 years. The response spectrum of the single accelerogram is reported by a grey line, the median spectrum is represented by a black line, whereas 84% and 16% percentile spectra are depicted by red lines. For the sake of comparison, the elastic spectrum provided by the Italian seismic code for soil type B with a 5% equivalent viscous damping ratio is also reported. The figure shows that the period of vibration corresponding to the maximum value of the pseudo acceleration (T_{max}) is smaller in the case of a vs. of 700 m/s.

Attention is particularly focused on the ratios of the spectral accelerations provided by the 50% percentile spectra obtained by the local seismic response analysis ($S_{a,50\%}$) to those provided by the Italian seismic code for soil type B ($S_{a,code}$). Specifically, the above ratios are plotted in Figure 5, with specific regard to three periods of vibration: (1) T = 0.0 s, (2) $T = T_{max}$, and (3) $T = T_1$, where T_1 is the first period of vibration of the structure determined, neglecting the soil–foundation interaction.

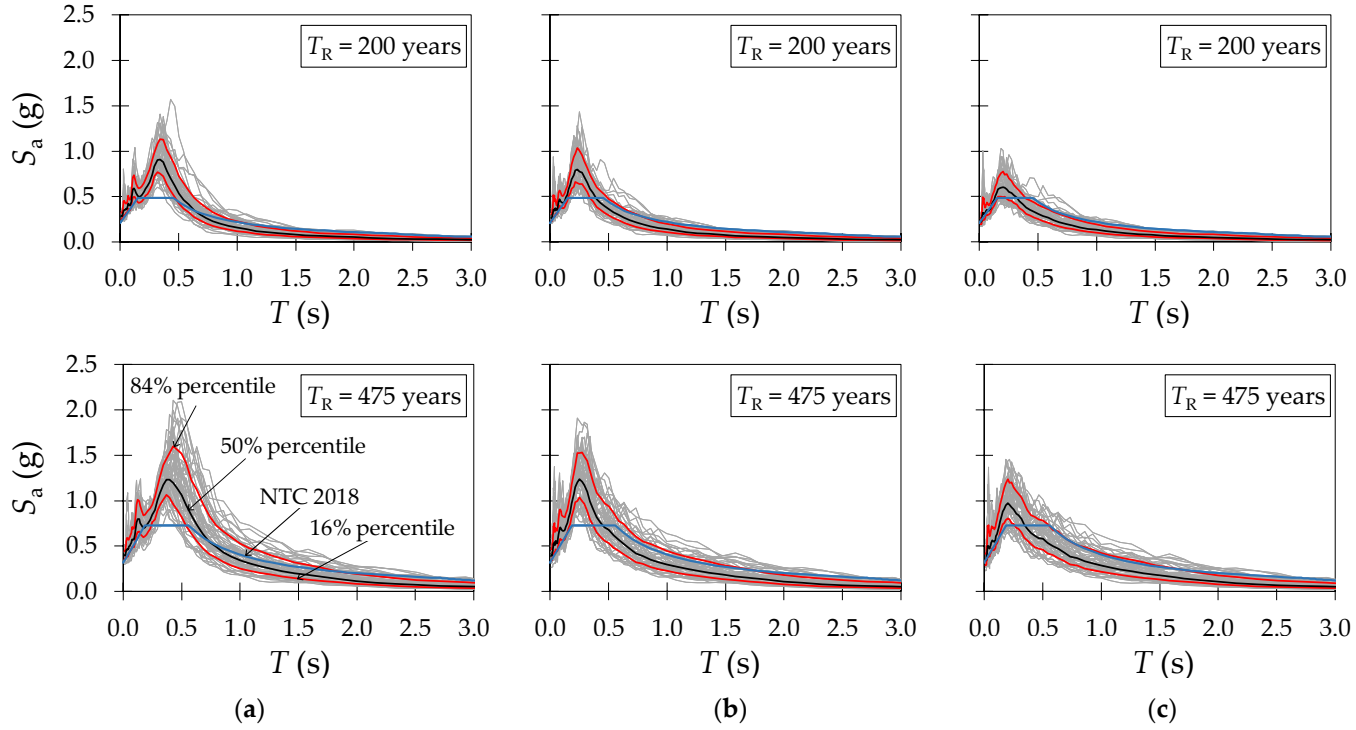


Figure 4. Spectra of the generated accelerograms: (**a**) V_s = 400 m/s; (**b**) V_s = 550 m/s; and (**c**) V_s = 700 m/s.

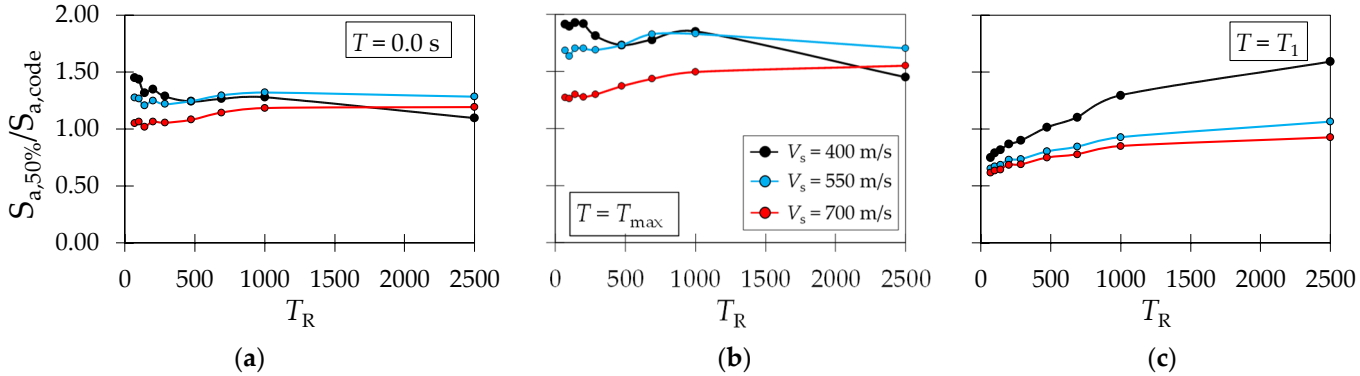


Figure 5. Ratios of the spectral acceleration at (**a**) T = 0.0 s; (**b**) $T = T_{max}$; and (**c**) $T = T_1$.

For low return periods (T_R up to 475 years), the smaller the equivalent shear wave velocity, the higher the amplification of the spectral accelerations at both T = 0.0 s and $T = T_{max}$. For longer return periods, instead, the amplifications of the spectral accelerations provided by the soil with V_s = 400 m/s and V_s = 550 m/s become similar, because the worst quality of the soil is partially balanced by the higher damping due to the increasing values of the shear deformation in the soil. The amplification of the spectral acceleration at $T = T_1$, instead, is always larger in the case of V_s = 400 m/s.

5. Numerical Model

Numerical models of half the building are built within the Opensees framework. A leaning column is introduced to simulate PΔ effects. The response of each case study is determined by two numerical models: in the first numerical model (M#1), the soil–foundation interaction is accounted for, whereas in the second model (M#2), it is neglected.

In keeping with the recommendations given in [40], braces are modeled by four nonlinear beam–column elements with three integration points per element. To simulate the effects of imperfections and, thus, to promote the out-of-plane buckling of the braces, a

camber equal to 0.1% the length of the brace is applied out-of-plane. Hence, as x and y are the axes in the plane of the structure, the z coordinates of the intermediate nodes of the braces are not null. In particular, the coordinates of intermediate nodes of the brace are arranged along a sinusoidal curve. Geometric nonlinearities of the braces are accounted for by means of the corotational formulation

The gusset plates at the two ends of the brace are modeled as proposed in [17]. In particular, the gusset plates are simulated by elastic beam–column elements with a rectangular cross-section $W \times t_p$. A rotational spring is added at the ends of the braces (Figure 5). The out-of-plane flexural stiffness and the plastic flexural resistance of the spring are determined according to Hisaio et al. [13].

The portions of the beams and columns stiffened by the gusset plates are simulated by the means of elastic elements that are represented by thick lines in Figure 6a,b. The area and moment of inertia of these elastic elements are determined considering an equivalent cross-section that includes the cross-section of the relevant element (beam or columns) and the effective portion of the gusset plate (see [17] for more details about the definition of the effective portion of the gusset plate and the modeling of braces). The beams and columns of the braced frames are modeled by elastic beam–column elements, whereas all the other beams and columns are modeled as *Beam with finite length hinge* elements. The steel 02 uniaxial material is assigned to fibers.

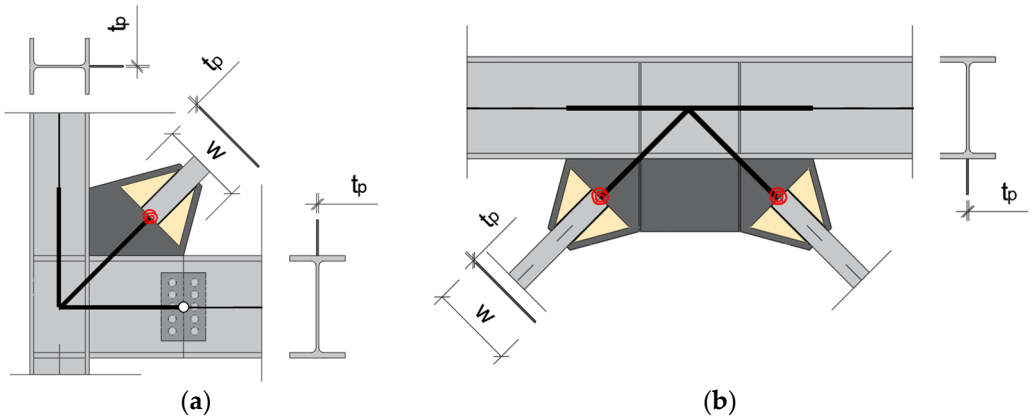


Figure 6. Details of the numerical models of the stiffening effect of the gusset plates at (**a**) the bottom and (**b**) the top of the brace.

In model M#1, the foundation is modeled by elastic beam–column elements. Intermediate nodes are disposed of in steps of 1.0 m. To account for the cracking of concrete, the elastic modulus is reduced by a factor equal to 0.5.

Horizontal and vertical zero-length elements are assigned at each of the nodes of the footings. The horizontal elements consist of a nonlinear spring and a dashpot acting in parallel. The steel 01 uniaxial material model is assigned to the horizontal spring: the stiffness of the spring is assigned to simulate the elastic soil sliding deformation, whereas the yielding force is equal to the friction limit between the soil and the foundation. The material QzSimple2 is assigned to the vertical zero elements. This material model allows for the simulation of both the nonlinear response of the soil and the effects of damping associated with the soil–foundation interaction.

The horizontal and vertical stiffness of the zero-length elements (k_H and k_v) and the radial damping (β_h and β_v) are calculated based on the proposal by Pais and Kausel [41]. In particular, k_H and k_V are calculated as the static stiffnesses of the entire foundation at zero frequency (K_H or K_V) times the dynamic stiffness modifiers (α_H and α_v) and divided by the number n of vertical springs in the model, where:

$$K_H = \frac{GB}{2-\nu}\left[6.8\left(\frac{L}{B}\right)^{0.65} + 2.4\right]; \quad K_V = \frac{GB}{1-\nu}\left[3.1\left(\frac{L}{B}\right)^{0.75} + 1.6\right] \tag{4}$$

$$\alpha_H = 1.0 \qquad \alpha_V = 1.0 - \frac{\left(0.4 + \frac{0.2}{L/B}\right) a_0^2}{\frac{10}{1+3(L/B-1)} + a_0^2} \tag{5}$$

In the equations above, ν is the Poisson's coefficient (equal to 0.35), G is the shear modulus reduced because of the shear deformations, and a_0 is the dimensionless frequency. In particular, G is calculated as 0.9 times the shear modulus at a small strain G_0 that, in turn, is calculated as a function of the shear wave velocity and the soil density ρ:

$$G_0 = \rho V_s^2 \tag{6}$$

The parameter a_0 is calculated as $\omega B/V_s$, where ω is set as equal to the frequency corresponding to the period associated with the first-mode period of vibration.

The radial damping β_H and β_v of each dashpot are calculated as:

$$\beta_H = \frac{4L/B}{K_H/(GB)} \frac{a_0}{2\alpha_H} \frac{1}{n} \qquad \beta_V = \frac{4\psi L/B}{K_V/(GB)} \frac{a_0}{2\alpha_V} \frac{1}{n} \tag{7}$$

where:

$$\psi = \sqrt{2(1-\nu)/(1-2\nu)} \leq 2.5 \tag{8}$$

The viscous damping terms c_H and c_V assigned to the horizontal dashpot and the QzSimple2 material are calculated as a function of the radial damping:

$$c_H = \frac{2\ \beta_H k_H}{\omega}, \qquad c_V = \frac{2\ \beta_V k_V}{\omega} \tag{9}$$

The sliding resistance V_H of the horizontal spring is calculated based on the vertical loads in the seismic design situation ($G_k + \psi_2 Q_{k\,=}$ 7.0 kN/m^2), and the friction angle φ' as:

$$V_H = \frac{[(G_k + \psi_2 Q_k) \cdot A + P_k] \tan \varphi'}{n} \tag{10}$$

where A is the area of half the building multiplied by the number of stories, P_k is the characteristic value of the self-weight of the strip foundation, and n is the number of horizontal springs in the model.

The ultimate capacity of the vertical spring is equal to the Brinch Hansen capacity Q_{ult} (evaluated assuming that $2L = 2L'$) divided by the number of vertical springs n. Finally, the displacement z_{50} at which 50% of the ultimate capacity is mobilized in monotonic loading is calculated as:

$$z_{50} = \frac{1.39\ Q_{ult}}{K_V \alpha_V} \tag{11}$$

where the coefficient 1.39 is suggested for sand based on the calibration of several shallow foundation test results [42]. Finally, the uplift resistance is set as equal to 5% of the ultimate capacity in compression.

6. Numerical Analyses and Response Parameters

The seismic response of the structures is investigated by multiple-stripe analysis. For each considered return period T_R of the seismic event, a different suite of 50 accelerograms is used as a seismic input, as reported in Section 4. The Rayleigh formulation is used to introduce damping. In particular, the stiffness and the mass proportional coefficients are computed so that the equivalent viscous damping ratio is equal to 3% for the first and second modes of vibration of the structure.

The intensity measure (IM) conventionally associated with the considered T_R is the peak ground acceleration on soil type B provided by the Italian seismic code (i.e., $S \times a_g$).

For a given intensity measure and for each accelerogram, both local and global response parameters are recorded. In particular, for dissipative members, i.e., for braces, the maximum ductility demands in tension and compression are calculated during the time

history as the ratio of the maximum elongation and shortening of the brace to the elongation at yield. The sum of the ductility demands in tension and compression is compared with the total ductility capacity μ_f that, according to Tremblay [43], is expressed as a function of the brace slenderness λ and the local slenderness of the cross-section. Specifically, in the case of hollow square cross-sections, the total ductility capacity is calculated as:

$$\mu_f = 1 + \theta_f^2 \frac{E_s}{2f_y} \quad \text{with } \theta_f = 0.091 \left(\frac{d}{t}\right)^{-0.2} \lambda^{0.3} \tag{12}$$

where d/t is the depth-to-thickness ratio.

The ductility demand and capacity are used to define a damage index DI that reaches 1.0 at brace failure, i.e.,

$$DI = \frac{\mu_d - 1}{\mu_f - 1} \tag{13}$$

Regarding fragile members, i.e., the beams and columns of the braced frames, the time history of bending moments $M_{Ed}(t)$ and axial forces $N_{Ed}(t)$ is recorded. Then, at each instant of time, resistance and stability indexes (RI and LSI) are determined starting from the relevant provisions given in Eurocode 3 and the maximum values of both indexes are calculated. A value of RI equal to 1.0 identifies yielding due to the combined effects of bending moments and axial forces; a value of LSI equal to 1.0, instead, identifies buckling of the member. In this regard, when beams are considered, buckling about the weak axis is considered to be prevented.

Finally, the maximum inter-story drifts (δ_{max}) and the residual drifts (δ_{res}) are determined.

The above response parameters are elaborated to obtain the fragility curves for the Damage Limitation (DL), Significant Damage (SD), and Near Collapse (NC) limit states. The association of the limit values of the response parameters with the relevant limit state is reported in Table 4. In the same table, the probability of exceedance P_{VR} in 50 years of the seismic event (and the associated return period) for which the fulfillment of the limit state is expected based on the provisions of the Italian seismic code is also reported.

Table 4. Limit values of the response parameters at the considered limit states.

Response Parameter	DL Limit State	SD Limit State	NC Limit State
δ_{max}	0.5% h *	1.5% h	2.0% h
δ_{res}	-	0.5% h	-
DI	0.25	0.75	1.00
RI	-	1.00	1.00
LSI	-	1.00	1.00
P_{VR} in 50 years	63% *	10%	5% **
T_R	50 years *	475 years	1000 years **

* δ_{max} = 0.75% h, P_{VR} = 35% in 50 years, and T_R = 115 years according to EC8; ** P_{VR} = 3% in 50 years and T_R = 1600 years according to EC8.

Each fragility curve [see Equation (14)] is expressed as a function of two parameters, θ and β, that represent the median intensity measure corresponding to the achievement of the considered limit state and the record-to-record uncertainty, respectively.

$$P(C|IM = s) = \Phi\left(\frac{\ln(s/\theta)}{\beta}\right) \tag{14}$$

In particular, parameters θ and β are obtained by maximizing the logarithm of the likelihood function, as reported in the following relationship [44]

$$\{\hat{\theta},\ \hat{\beta}\} = \underset{\theta,\ \beta}{\operatorname{argmax}} \sum_{j=1}^{m} \left\{ \ln\binom{n_j}{z_j} + z_j \ln \Phi\left(\frac{\ln(s_j/\theta)}{\beta}\right) + (n_j - z_j) \ln\left[1 - \Phi\left(\frac{\ln(s_j/\theta)}{\beta}\right)\right] \right\} \tag{15}$$

where n_j is the number of analyses that have been carried out at the intensity measure IM = s_j and z_j is the number of analyses in which the considered limit state has been exceeded.

7. Influence of Modeling of Soil–Foundation Interaction on Seismic Performance

In order to assess the influence of the modeling of the soil–foundation interaction on the assessment of the seismic response, fragility curves derived based on the results obtained by the numerical analyses carried out on models M#1 and M#2 are compared. Similar trends are observed for structures standing on soils with different shear wave velocities; hence, only results referring to structures standing on soil with V_s = 400 m/s are reported here. In particular, no significant influence of the explicit modeling of the soil–foundation interaction is recorded in terms of inter-story drifts (Figure 7a), the DI of braces (Figure 7b), and the LSI of columns (Figure 7c). The modeling of the soil–foundation flexibility does not affect the response of the structure due to the continuity of the strip foundation under multiple columns and the presence of hinges between the foundation and the columns.

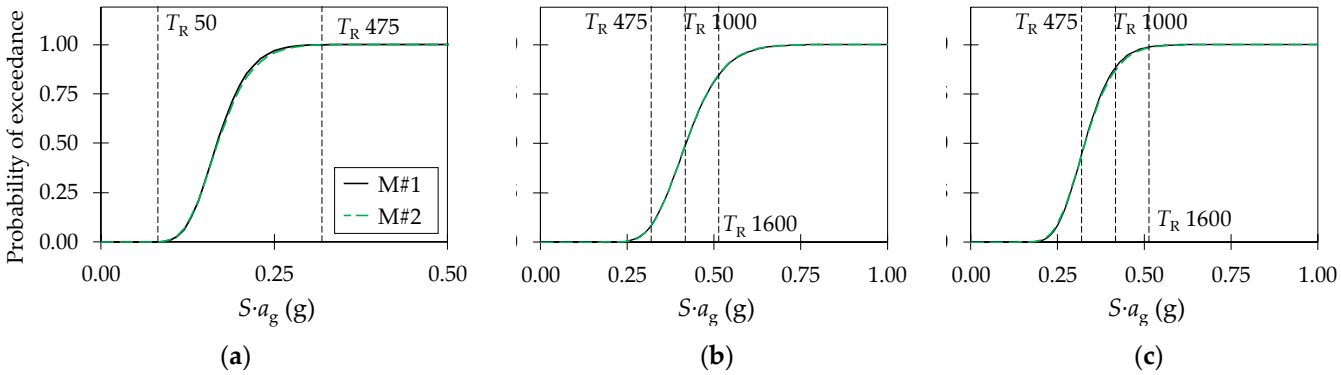


Figure 7. Comparison of fragility obtained either modeling or neglecting the soil–foundation interaction in the case of (**a**) drifts at the DL limit state, (**b**) DI of braces at the SD limit state, and (**c**) LSI of columns at the NC limit state (V_s = 400 m/s).

Based on the above results, in the following section, only the results obtained for model M#1 will be discussed.

8. Effectiveness of Design Procedure of Upcoming Version of Eurocode 8

The analysis of the fragility curves in terms of inter-story drifts (Figure 8) shows that the structures designed according to the upcoming version of Eurocode 8 have an almost null probability of exceedance of a value of the maximum inter-story drift equal to 0.5% h for seismic events with T_R = 50 years. For a seismic event with T_R = 475 years, the probability of exceedance of the maximum inter-story drift provided by Eurocode 8 (i.e., 1.5% h) ranges from 0.12% to 0.23%. The smallest probability of exceedance occurs for the structure standing on soil with V_s = 700 m/s. Finally, in all the considered cases, the probability of exceedance for a value of the maximum inter-story drift equal to 2.0% h (assumed as the limit value at the NC limit state in FEMA356) is lower than 50% for seismic events with T_R = 1000 years and higher than 50% for seismic events with T_R = 1600 years.

Similarly, the probability of exceedance of a DI for braces equal to 0.75 for seismic events with T_R = 475 years is in the range from 5% to 9% (Figure 9a); the probability of exceedance of DI = 1.00 (i.e., the limit value at the NC limit state) is significantly smaller than 50% for T_R = 1000 years (i.e., the return period associated with the NC limit state in the Italian seismic code), whereas it is larger than 50% for seismic events with T_R = 1600 years (the return period associated with the NC limit state in Eurocode 8 for structures belonging to consequence class 2) only in the case of the structure standing on soil with V_s = 400 m/s (Figure 9b).

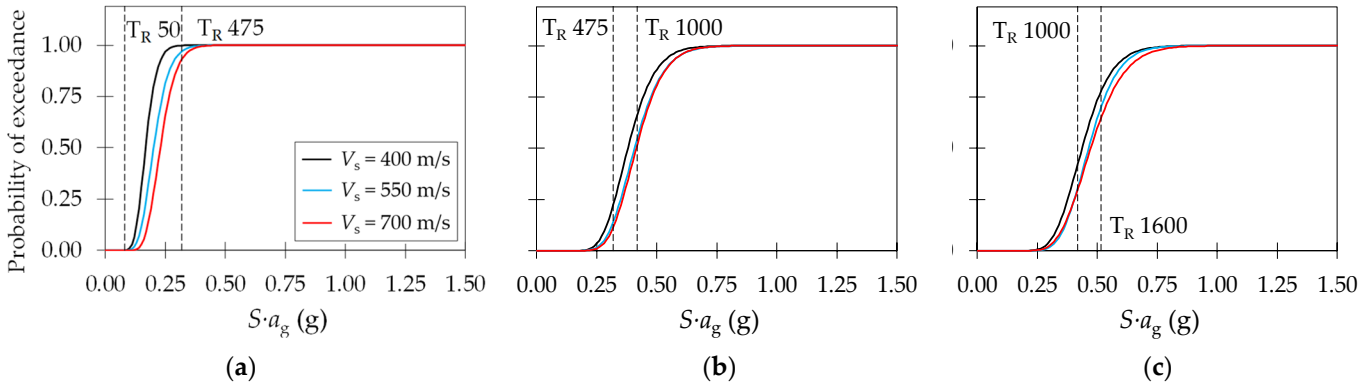


Figure 8. Fragility curves in terms of maximum drifts at (**a**) DL, (**b**) SD, and (**c**) NC limit states.

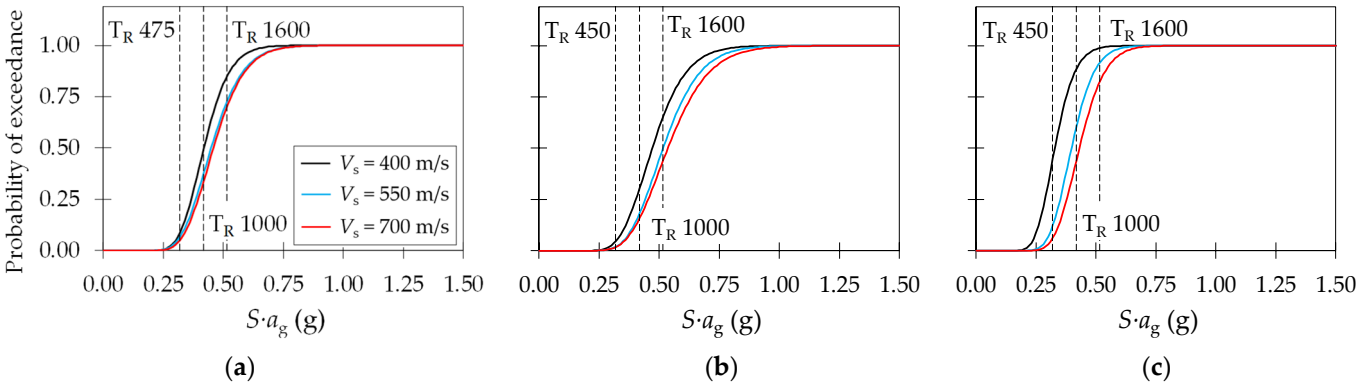


Figure 9. Fragility curves in terms of (**a**) DI of braces at SD and (**b**) NC limit state; (**c**) LSI of columns.

The achievement of a value of the LSI for columns equal to 1.0 has a probability of exceedance smaller than 50% in the case of T_R = 475 and larger than 50% in the case of T_R = 1000 years (Figure 9c). Hence, the rules for the application of the capacity design principles provided in the upcoming version of Eurocode 8 are able to guarantee a significantly improved performance of columns with respect to that of columns in structures designed according to the previous version of Eurocode 8 [11]. Despite this improvement, mainly related to a better estimation of the bending moments in columns, the premature buckling of columns still occurs.

In addition, Figs. 8 and 9 highlight that the fragility curves for V_s = 550 m/s and 700 m/s are very similar to each other. In these cases, as the mobilized shear strain levels and, thus, the corresponding shear modulus and damping ratio of the soil are similar, soil-filtering effects lead to a similar amplification of the seismic input. On the other hand, for a lower shear wave velocity (V_s = 400 m/s), the soil-filtering effects mobilize a greater shear strain level and so lead to a lower shear modulus and higher damping ratio, with a prevalent effect of the lower shear modulus. This leads to a more remarkable amplification of the seismic input compared with the previous cases. The achieved results suggest that the shear wave velocity range provided by the current Eurocode 8 and Italian Seismic code for soil type B is too large and needs to be revised.

9. Conclusions

Three buildings with concentric bracings in the chevron configuration were designed according to the design procedure reported in the upcoming version of Eurocode 8. The three case studies differed because of the values of the shear wave velocity of the site under consideration. Specifically, shear wave velocity values equal to either 400, 550, or 700 m/s were considered. A strip foundation was designed for each case study.

The seismic performance of the considered buildings was assessed in terms of fragility curves, referring to Damage Limitation, Significant Damage, and Near Collapse limit states.

The response parameters used to assess the performance were inter-story drifts, the damage index of braces, and the resistance and stability indexes of fragile members (i.e., braced beams and columns).

The data used to compute the fragility curves were derived by multiple-stripe analyses carried out on refined numerical models that properly reproduced the cyclic response of braces and that either took into account or neglected the soil–foundation flexibility.

The seismic input was determined based on a local seismic response analysis carried out on the considered soils. Based on the results obtained, it was concluded that:

- The assessment of the seismic performance of the considered case studies was not affected by the modeling of the soil–foundation flexibility due to the continuity of the strip foundation under multiple columns and the presence of hinges between the foundation and columns. Different foundation types will be explored in the future to further investigate the influence of the modeling of the soil–foundation flexibility.
- The shear wave velocity range provided by the current Eurocode 8 and Italian Seismic code for soil type B, equal to 360–800 m/s, is too large and needs to be revised.
- The use of a one-dimensional local site response analysis to properly take into account the soil-filtering effects was of paramount importance to define the seismic input. Indeed, the fragility curves derived for the case study standing on a soil with V_S = 400 m/s provided probabilities of exceedance of the considered limit states significantly higher than those provided by the fragility curves derived in the case of V_S = 550 and 700 m/s. This was due to the greater shear strain level and, consequently, to the lower shear modulus and higher damping ratio, with a prevalent effect of the lower shear modulus, mobilized for the lowest investigated V_S. This led to a more remarkable amplification of the seismic input compared with the other cases.
- The design procedure reported in the upcoming version of Eurocode 8 for concentrically braced frames in the chevron configuration leads to structures that provide a reasonably low probability of exceedance of the considered limit states in terms of inter-story drifts and the damage index of braces. When the stability of columns was considered as a response parameter, however, the probability of exceedance was smaller than 50% in the case of seismic events with an intensity measure associated with the Significant Damage limit state and larger than 50% in the case of seismic events with an intensity measure associated with the Near Collapse limit state.

Author Contributions: Conceptualization, M.B., A.F., M.R.M. and P.P.R.; methodology, M.B., A.F., M.R.M. and P.P.R.; formal analysis, M.B., A.F., M.R.M. and P.P.R.; investigation, M.B., A.F., M.R.M. and P.P.R.; writing—review and editing, M.B., A.F., M.R.M. and P.P.R. All authors have read and agreed to the published version of the manuscript.

Funding: This research received no external funding.

Data Availability Statement: The raw data supporting the conclusions of this article will be made available by the authors on request.

Conflicts of Interest: The authors declare no conflicts of interest.

References

1. *CEN. EN 1998-1*; EuroCode 8: Design of Structures for Earthquake Resistance–Part 1: General Rules, Seismic Actions and Rules for Buildings. European Committee for Standardization: Bruxelles, Belgium, 2004.
2. D'Aniello, M.; Costanzo, S.; Landolfo, R. The influence of beam stiffness on seismic response of chevron concentric bracings. *J. Constr. Steel Res.* **2015**, *112*, 305–324. [CrossRef]
3. Marino, E.M. A unified approach for the design of high ductility steel frames with concentric braces in the framework of Eurocode 8. *Earthq. Eng. Struct. Dyn.* **2014**, *43*, 97–118. [CrossRef]
4. Bosco, M.; Brandonisio, G.; Marino, E.M.; Mele, E.; De Luca, A. Ω* method: An alternative to Eurocode 8 procedure for seismic design of X-CBFs. *J. Constr. Steel Res.* **2017**, *134*, 135–147. [CrossRef]
5. Costanzo, S.; D'Aniello, M.; Landolfo, R. Seismic design criteria for chevron CBFs: Proposals for the next EC8 (part-2). *J. Constr. Steel Res.* **2017**, *138*, 17–37. [CrossRef]

6. Azad, S.K.; Topkaya, C.; Astaneh-Asl, A. Seismic behavior of concentrically braced frames designed to AISC341 and EC8 pro-visions. *J. Constr. Steel Res.* **2017**, *133*, 383–404. [CrossRef]
7. Longo, A.; Montuori, R.; Piluso, V. Plastic Design of Seismic Resistant V-Braced Frames. *J. Earthq. Eng.* **2008**, *12*, 1246–1266. [CrossRef]
8. Longo, A.; Montuori, R.; Piluso, V. Seismic reliability of V-braced frames: Influence of design methodologies. *Earthq. Eng. Struct. Dyn.* **2009**, *38*, 1587–1608. [CrossRef]
9. Wang, Y.D.; Nastri, E.; Tirca, L.; Montuori, R.; Piluso, V. Comparative Response of Earthquake Resistant CBF Buildings Designed according to Canadian and European Code Provisions. *Key Eng. Mater.* **2018**, *763*, 1155–1163. [CrossRef]
10. Kumar, P.C.A.; Anand, S.; Sahoo, D.R. Modified seismic design of concentrically braced frames considering flexural demand on columns. *Earthq. Eng. Struct. Dyn.* **2017**, *46*, 1559–1580. [CrossRef]
11. Barbagallo, F.; Bosco, M.; Marino, E.M.; Rossi, P.P. Proposal and validation of a design procedure for concentrically braced frames in the chevron configuration. *Earthq. Eng. Struct. Dyn.* **2021**, *50*, 3041–3063. [CrossRef]
12. Roeder, C.W.; Sen, A.D.; Terpstra, C.; Ibarra, S.M.; Liu, R.; Lehman, D.E.; Berman, J.W. Effect of beam yielding on chevron braced frames. *J. Constr. Steel Res.* **2019**, *159*, 428–441. [CrossRef]
13. Hsiao, P.-C.; Lehman, D.E.; Roeder, C.W. Improved analytical model for special concentrically braced frames. *J. Constr. Steel Res.* **2012**, *73*, 80–94. [CrossRef]
14. *prEN_1998-1-2_2022_ENQ*; Eurocode 8: Earthquake Resistance Design of Structures. British Standard: London, UK, 2005.
15. D'Aniello, M.; Ambrosino, G.L.M.; Portioli, F.; Landolfo, R. The influence of out-of-straightness imperfection in physical theory models of bracing members on seismic performance assessment of concentric braced structures. *Struct. Des. Tall Spec. Build.* **2014**, *24*, 176–197. [CrossRef]
16. Silva, A.; Castro, J.M.; Monteiro, R. Brace-to-frame connection modelling effects on seismic loss assessment of steel concentrically-braced frames. *J. Constr. Steel Res.* **2020**, *172*, 10623. [CrossRef]
17. Bosco, M. Influence of uncertainties on the seismic performance assessment of chevron braced frames. *Eng. Struct.* **2023**, *294*, 116594. [CrossRef]
18. Montuori, R.; Nastri, E.; Piluso, V.; Todisco, P. The effect of the gravity column in the seismic design of steel CBFs. *Structures* **2023**, *57*, 105229. [CrossRef]
19. Tuladhar, R.; Maki, T.; Mutsuyoshi, H. Cyclic behavior of laterally loaded concrete piles embedded into cohesive soil. *Earthq. Eng. Struct. Dyn.* **2008**, *37*, 43–59. [CrossRef]
20. Officially the Italian Republic. NTC 2018. D.M. 17/01/18—Updating of Technical Standards for Buildings. 2018, 42. Available online: https://www.gazzettaufficiale.it/eli/gu/2018/02/20/42/so/8/sg/pdf (accessed on 19 January 2024).
21. Mylonakis, G.; Gazetas, G.; Nikolaou, S.; Michaelides, O. The Role of Soil on the Collapse of 18 Piers of the Hanshin Expressway in the Kobe Earthquake. In Proceedings of the 12th World Conference on Earthquake Engineering, Auckland, New Zealand, 30 January–4 February 2000. Paper No. 1074.
22. Labbé, P.; Paolucci, R. Developments Relating to Seismic Action in the Eurocode 8 of Next Generation. *Springer Proc. Earth Environ. Sci.* **2022**, 26–46. [CrossRef]
23. Hernández-Aguirre, V.M.; Paolucci, R.; Sánchez-Sesma, F.J.; Mazzieri, I. Three-dimensional numerical modeling of ground motion in the Valley of Mexico: A case study from the Mw3.2 earthquake of July 17, 2019. *Earthq. Spectra* **2023**, *39*, 2323–2351. [CrossRef]
24. Pitilakis, K.; Riga, E.; Anastasiadis, A. New code site classification, amplification factors and normalized response spectra based on a worldwide ground-motion database. *Bull. Earthq. Eng.* **2013**, *11*, 925–966. [CrossRef]
25. Massimino, M.R.; Abate, G.; Corsico, S.; Louarn, R. Comparison Between Two Approaches for Non-linear FEM Modelling of the Seismic Behaviour of a Coupled Soil-Structure System. *Geotech. Geol. Eng.* **2019**, *37*, 1957–1975. [CrossRef]
26. Abate, G.; Corsico, S.; Fiamingo, A.; Grasso, S.; Massimino, M.R. Evaluation of DSSI for the preservation of the Catania University Central Palace. In *Geotechnical Engineering for the Preservation of Monuments and Historic Sites*, 3rd ed.; Lancellotta, R., Viggiani, C., Flora, A., de Silva, F., Mele, L., Eds.; CRC Press/Balkema: Boca Raton, FL, USA, 2022; pp. 823–835.
27. Abate, G.; Fiamingo, A.; Massimino, M.R. Sustainable Building: The Role of the Soil Parameters on Earthquake Safety. In *Lecture Notes in Civil Engineering*; Zembaty, Z., Perkowski, Z., Beben, D., Massimino, M.R., Lavan, O., Eds.; Springer Science and Business Media: Berlin, Germany, 2023; Volume 322, pp. 32–47.
28. Andreotti, G.; Famà, A.; Lai, C.G. Hazard-dependent soil factors for site-specific elastic acceleration response spectra of Italian and European seismic building codes. *Bull. Earthq. Eng.* **2018**, *16*, 5769–5800. [CrossRef]
29. Paolucci, R.; Aimar, M.; Ciancimino, A.; Dotti, M.; Foti, S.; Lanzano, G.; Mattevi, P.; Pacor, F.; Vanini, M. Checking the site categorization criteria and amplification factors of the 2021 draft of Eurocode 8 Part 1–1. *Bull. Earthq. Eng.* **2021**, *19*, 4199–4234. [CrossRef]
30. Wichman, S.; Berman, J.W.; Lehman, D.E.; Star, L.; Moresco, J. Factors affecting the seismic collapse performance of realistic low-rise braced frame buildings, including soil structure interaction and foundation flexibility. *Earthq. Eng. Struct. Dyn.* **2022**, *51*, 2335–2356. [CrossRef]
31. Vessia, G.; Laurenzano, G.; Pagliaroli, A.; Pilz, M. Seismic site response estimation for microzonation studies promoting the resilience of urban centers. *Eng. Geol.* **2021**, *284*, 106031. [CrossRef]
32. Chiaradonna, A.; Karakan, E.; Lanzo, G.; Monaco, P.; Sezer, A.; Karray, M. Influence of Local Soil Conditions on the Damage Distribution in Izmir Bay during the October 30, 2020, Samos Earthquake. *Geotec. Geol. Earthq. Eng.* **2022**, *52*, 871–878.

33. Cavallaro, A.; Fiamingo, A.; Grasso, S.; Massimino, M.R.; Sammito, M.S.V. Local site amplification maps for the volcanic area of Trecastagni, south-eastern Sicily (Italy). *Bull. Earthq. Eng.* **2024**, *22*, 1635–1676. [CrossRef]
34. Stewart, J.P.; Seed, R.B.; Fenves, G.L. *Empirical Evaluation of Inertial Soil-Structure Interaction Effects*; PEER Report 1998/07; Pacific Earthquake Engineering Research Center: Berkeley, CA, USA, 1998.
35. Brinch Hansen, J. The philosophy of foundation design: Criteria, safety factors and settlement limits. In Proceedings of the Symp. on Bearing Capacity and Settlements of Found., Roorkee, India, 24–26 February 1964.
36. Barbagallo, F.; Bosco, M.; Marino, E.; Rossi, P. Variable vs. invariable elastic response spectrum shapes: Impact on the mean annual frequency of exceedance of limit states. *Eng. Struct.* **2020**, *214*, 110620. [CrossRef]
37. Vanmarcke, E.H.; Gasparini, D.A. *A Program for Artificial Motion Generation, User's Manual and Documentation*; Department of Civil Engineering MIT: Cambridge, MA, USA, 1976.
38. Kottke, A.R.; Rathje, E.M. *Technical Manual for Strata Version 0.2.0*; University of Texas: Austin, TX, USA, 2010.
39. Darendeli, M.B. Development of a New Family of Normalized Modulus Reduction and Material Damping Curves. Ph.D. Dissertation, The University of Texas at Austin, Austin, TX, USA, 2001.
40. Uriz, P.; Filippou, F.C.; Mahin, S.A. Model for Cyclic Inelastic Buckling of Steel Braces. *J. Struct. Eng. (ASCE)* **2008**, *134*, 619–628. [CrossRef]
41. Pais, A.; Kausel, E. Approximate formulas for dynamic stiffnesses of rigid foundations. *Soil Dyn. Earthq. Eng.* **1988**, *7*, 213–227. [CrossRef]
42. Raychowdhury, P. Nonlinear Winkler-Based Shallow Foundation Model for Performance Assessment of Seismically Loaded Structures. Ph.D. Thesis, University of California, San Diego, CA, USA, 2008.
43. Tremblay, R.; Archambault, M.-H.; Filiatrault, A. Seismic Response of Concentrically Braced Steel Frames Made with Rectangular Hollow Bracing Members. *J. Struct. Eng.* **2003**, *129*, 1626–1636. [CrossRef]
44. Baker, J.W. Efficient Analytical Fragility Function Fitting Using Dynamic Structural Analysis. *Earthq. Spectra* **2015**, *31*, 579–599. [CrossRef]

Disclaimer/Publisher's Note: The statements, opinions and data contained in all publications are solely those of the individual author(s) and contributor(s) and not of MDPI and/or the editor(s). MDPI and/or the editor(s) disclaim responsibility for any injury to people or property resulting from any ideas, methods, instructions or products referred to in the content.